Available online at www.sciencedirect.com
ScienceDirect
Ceramics International 38 (2012) 119–124
CERAMICS INTERNATIONAL
www.elsevier.com/locate/ceramint

Microstructure and optical properties of electrodeposited Al-doped ZnO nanosheets

Yuan-Chang Liang *

Institute of Materials Engineering, National Taiwan Ocean University, Keelung 20224, Taiwan

Received 7 December 2010; received in revised form 18 April 2011; accepted 3 May 2011
Available online 25th June 2011

Abstract

This study grew A1-doped ZnO nanosheets on polycrystalline zinc foils using cathodic electrodeposition in an aqueous solution consisting of 0.02 M $Zn(NO_3)_2$ and 0.001 M $Al(NO_3)_3$ at 90 °C. The effects of the electrodepositing potential and thermal annealing on the physical properties of the Al-doped ZnO sheets were investigated. This study observed a high quality sheet-like structure of the electrodeposited Al-doped ZnO for the applied potential larger than −1.1 V, and the sheets were interconnected over the area of interest. The X-ray diffraction patterns showed that the intensity of the Bragg reflections of the electrodeposited Al-doped ZnO sheets increases with the electrodepositing potential because a larger applied potential results in the Al-doped ZnO sheets having a larger lateral dimension and thickness. However, the appearance of the Al-doped ZnO sheets becomes coarse and rough after thermal annealing at 400 °C in ambient air for 4 h. The intensity of the Bragg reflections of the Al-doped ZnO sheets was markedly increased through the thermal annealing due to the improvement of the crystalline quality of the annealed Al-doped ZnO sheets. Annealing caused a large decrease in structural defects of the Al-doped ZnO sheets electrodeposited at −1.3 V causing the sheets to exhibit a sharp photoluminescence peak at ∼380 nm.

Keywords: B. Defects; B. X-ray methods; C. Optical properties; D. ZnO

1. Introduction

Impurity-doped ZnO has attracted considerable attention due to its potential in nanodevice fabrication [1]. Several studies have used dopants to modify the electrical and optical properties of ZnO [2,3]. Al is a widely used Group III dopant. Al-doped ZnO is reported to be a useful material for a variety of technological applications [4,5]. Recently, the synthesis of nanostructured ZnO with various morphologies is widely developed due to versatile physical properties that are essential in various fields for applications such as sensors and solar cells [6–10]. Among diverse morphologies, the ZnO nanosheet was reported to have an advantage on a large surface area exposed to the environment; therefore, it is a promising medium for the fabrication of high-efficiency devices [11].

The ZnO nanostructures have been prepared using numerous methods [12–14]. Among various preparation methods, the electrochemical deposition has been widely adopted for the preparation of ZnO nanostructures due to advantages of high growth rate, large area, and low cost. The syntheses of ZnO nanosheets using electrodeposition on various substrates have been realized by several studies [11,15]; nevertheless, literature on the physical properties of ZnO nanosheets and related works on impurity-doped ZnO nanosheets is limited. The physical properties of Al-doped ZnO nanosheets prepared using electrodeposition have not been thoroughly examined. This work formed Al-doped ZnO nanosheets using electrodeposition, and investigated the effects of Al content and post-annealing on the physical properties of Al-doped ZnO nanosheets.

2. Experimental details

Al-doped ZnO nanosheets were grown by cathodic electrochemical deposition from an electrolyte containing 0.02 M $Zn(NO_3)_2$ and 0.001 M $Al(NO_3)_3$. The bath temperature is maintained at 90 °C during the electrodeposition of the Al-doped ZnO nanostructures. A standard three-electrode

* Tel.: +886 2 24622192; fax: +886 2 24625324.
E-mail address: yuanvictory@gmail.com.

0272-8842/$36.00
doi:10.1016/j.ceramint.2011.05.154

compartment cell was used in this experiment. A platinum sheet (99.99% purity) and a zinc foil (99.99% purity) were used as the anode and cathode, respectively. A Ag/AgCl electrode in a saturated KCl solution was used as a reference electrode. The area of the zinc foil in the electrolyte for the electrodeposition is fixed at 1 cm^2. The deposition was performed at various potentials from −0.9 V to −1.3 V with respect to the reference electrode. The as-grown samples were washed with deionized water and absolute ethanol several times. Some of the as-electrodeposited Al-doped ZnO nanostructures are subsequently annealed at 400 °C in air ambient for 4 h to evaluate the annealing effects on the structure and optical properties of the Al-doped ZnO nanostructures.

The crystal structure of the electrodeposited Al-doped ZnO nanostructures was characterized by X-ray diffraction (XRD) with Cu Kα radiation. The surface morphology and composition of the electrodeposited ZnO nanostructures was investigated by a scanning electron microscope (SEM), equipped with X-ray energy dispersive spectroscope (EDS). X-ray photoelectron spectroscope (XPS) measurements were performed to evaluate the binding state of oxygen in the Al-doped ZnO nanostructures. The room temperature dependent photoluminescence (PL) spectra are obtained using the 325 nm line of a He–Cd laser.

3. Results and discussion

Figs. 1(a)–(c) shows the surface morphologies of the electrodeposited Al-doped ZnO sheets on zinc foils under various potentials. The lateral dimension of the Al-doped ZnO sheets grown at −0.9 V is ∼0.4 μm, and the morphology of the sheets is not completely developed (Fig. 1(a)). Increasing the potential to −1.1 V resulted in a lateral dimension of approximately 0.8 μm and a thickness of tens of nanometers of the as-grown sheets (Fig. 1(b)). Further increasing the potential to −1.3 V, the dimension and thickness of the sheets increased considerably (Fig. 1(c)). The lateral dimension of the sheets reaches ∼1.8 μm and the sheets are almost vertical to the substrate. A high quality sheet-like structure of the electrodeposited Al-doped ZnO was observed for the applied potential larger than −1.1 V, and the sheets were interconnected over the area of interest. The ZnO sheets were prepared in a $Zn(NO_3)_2$ solution with an addition of KCl [13]. Small variations in the potentials during the electrochemical deposition were proved to give rise to a variety of surface morphologies of the ZnO. A two-dimensional sheet-like structure might form during electrochemical deposition as a transition between one-dimensional and three-dimensional growth of the electrodeposited ZnO [16]. Figs. 1(d)–(f) displays the surface morphologies of the Al-doped ZnO sheets annealed in ambient air for 4 h. The periphery of the annealed Al-doped ZnO sheets is not as sharp as those that are as-deposited. The appearance of the Al-doped ZnO sheets becomes coarse and rough after thermal annealing. The effect of thermal annealing on the deterioration of sheet morphology of the electrodeposited ZnO corresponds with previous work [17].

Fig. 2 shows the representative EDS patterns of the Al-doped ZnO sheets grown at −1.3 V. Oxygen, Zn, and Al peaks at ∼0.53, 1.0, and 1.5 keV, respectively, as shown in Fig. 2. The EDS result indicates that the dopant Al entered the lattice of the ZnO sheets during the electrodeposition. The atomic ratio of the constituent elements of the Al-doped ZnO was obtained using EDS, as shown in Table 1. The atomic concentration of Al in the ZnO matrix increased with the decreasing potential. This corresponds with Kemell et al. and is attributed to the fact that the formation of aluminum hydroxide is thermodynamically more favorable than that of zinc hydroxide during electrochemical deposition from the mixed solution of zinc nitrate and aluminum nitrate [18]. The atomic concentration of Al in the ZnO matrix electrodeposited at −0.9 V is 9.59%; this high Al concentration might indicate that some of the aluminum apparent in the sheets was amorphous alumina or AlO (OH).

Fig. 3 shows the XPS spectra of O 1s peaks of the as-electrodeposited and annealed Al-doped ZnO sheets. The O 1s

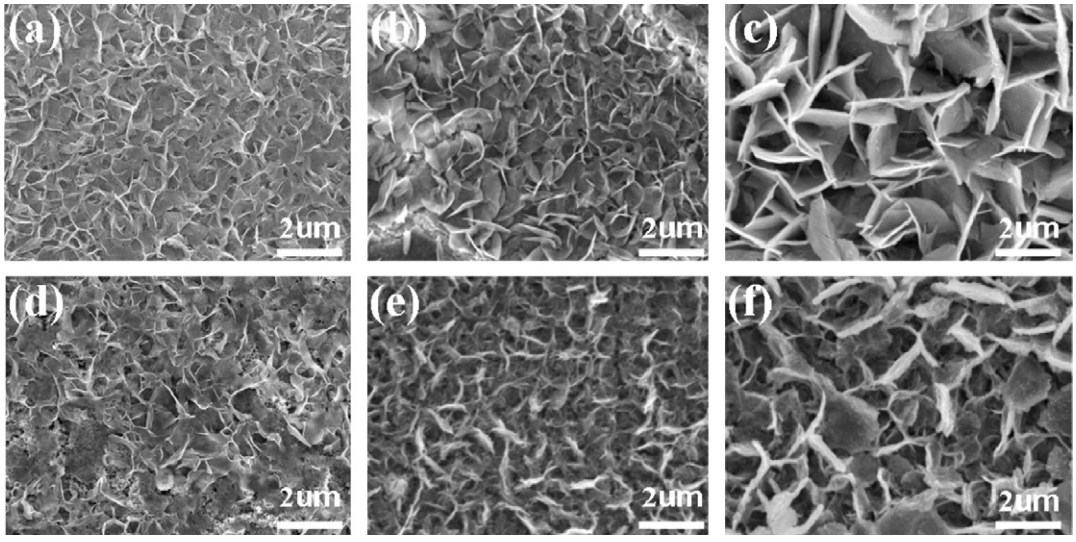

Fig. 1. SEM images of the electrodeposited Al-doped ZnO sheets grown at various potentials: (a) −0.9 V, (b) −1.1 V, and (c) −1.3 V. The surface morphology of the annealed sheets were shown in (d)–(f): (d) −0.9 V, (e) −1.1 V, and (f) −1.3 V.

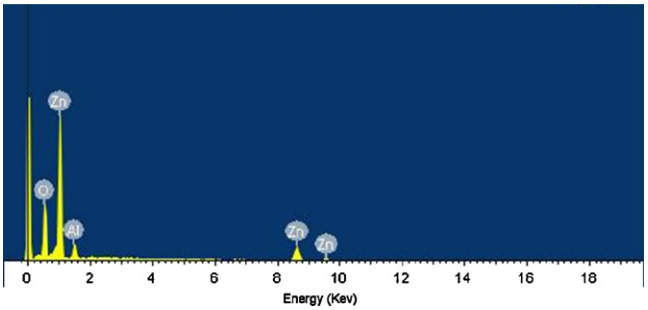

Fig. 2. EDS spectra of the electrodeposited Al-doped ZnO sheets electrodeposited at −1.3 V.

Table 1
Atomic ratio composition of the constituent elements in Al-doped ZnO sheets measured by EDS.

	Al	Zn	O	Al/(Al + Zn)
−0.9 V	9.59%	36.98%	53.43%	0.21
−1.1 V	5.20%	39.90%	54.90%	0.12
−1.3 V	3.78%	41.74%	54.48%	0.08

peaks were fitted by two Gaussian curves, centered at ∼530.25 and 531.25 eV. The component of the O 1s spectrum at 530.25 eV is associated with O^{2-} ions on a wurtzite structure of ZnO [19], and the higher peak area of this component within the O 1s spectrum represents the larger amount of oxygen atoms in a fully oxidized stoichiometric surrounding. The binding energy component, centered at 531.25 eV is close to the O1 s binding energy for AlO(OH) [20]. The existence of hydroxide in the sheets is due to the samples being prepared in an aqueous solution. The binding energy of the thermal annealed Al-doped ZnO sheets is lower than that without thermal annealing at a particular electrodeposition potential. This might be due to the reduced material disorder in the annealed Al-doped ZnO sheets.

Fig. 4 displays the XRD patterns for the electrodeposited Al-doped ZnO sheets on the zinc foils before and after thermal annealing. The XRD patterns of the Al-doped ZnO sheets prepared under various potentials consist of (1 0 0) (0 0 2) (1 0 1) (1 0 2), and (1 1 0) Bragg reflections from hexagonal ZnO JCPDS 36-1451 (Fig. 4(a)). These XRD patterns can be indexed as hexagonal wurtzite structures of ZnO. The intensity of the Bragg reflections of the electrodeposited Al-doped ZnO sheets increases with the depositing potential. The SEM images show that the size of the Al-doped ZnO sheets increases with the depositing potential. The larger lateral dimension and thickness of the Al-doped ZnO sheets were formed at a larger applied potential; this contributed to a higher intensity of the Bragg reflections of the Al-doped ZnO sheets. Moreover, the extrinsic Al^{3+} quickly absorbs more oxygen with a higher Al concentration in the ZnO sheets electrodeposited at a lower potential. This might result in the Al-doped ZnO sheets having a poor crystalline quality [21]. Notably, the angle position of the Bragg reflections of the Al-doped ZnO sheets varied with changes in the applied potential (Fig. 4(b)). The magnified XRD patterns of the (0 0 2) Bragg reflections of the Al-doped ZnO sheets grown at various potentials clearly reveal that the Bragg reflection shifts to a higher diffraction angle with an increase of growth potential from −0.9 to −1.1 V. Moreover, the diffraction angle of the ZnO (0 0 2) was reduced when the potential was further increased to −1.3 V. The shift of the XRD peaks was also observed while incorporating transition metals into ZnO crystalline [22]. The radius of Al^{3+}(54 pm) is slightly lower than that of Zn^{2+}(74 pm). Therefore, the incorporation of

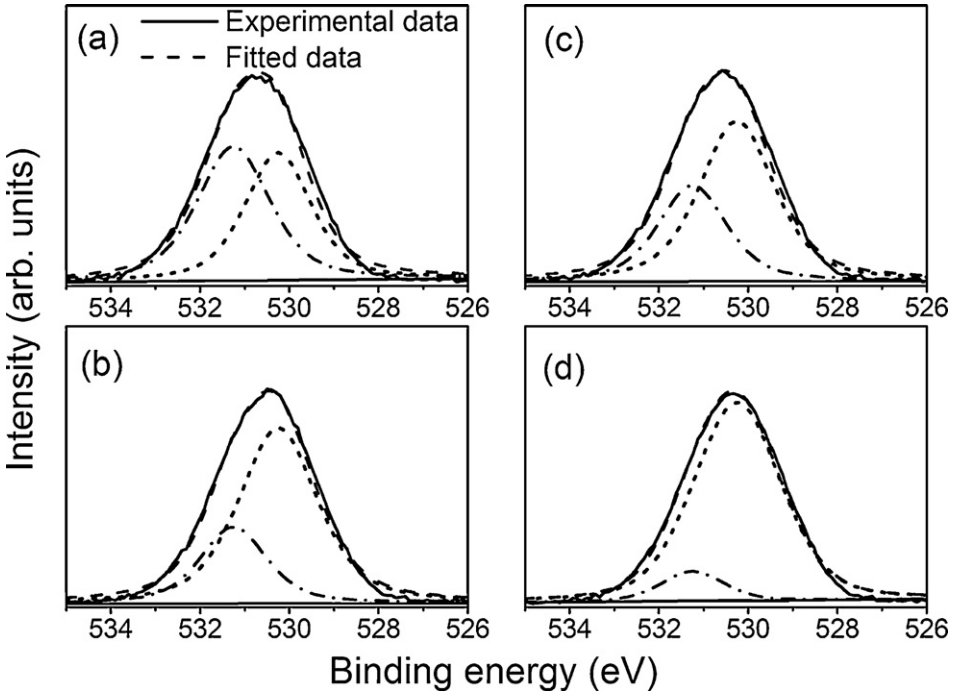

Fig. 3. The representative XPS spectra of the O 1s for the electrodeposited Al-doped ZnO sheets: (a) electrodeposited at −0.9 V, (b) electrodeposited at −0.9 V and annealed in air ambient at 400 °C for 4 h, (c) electrodeposited at −1.3 V, and (d) electrodeposited at −1.3 V and annealed in air ambient at 400 °C for 4 h.

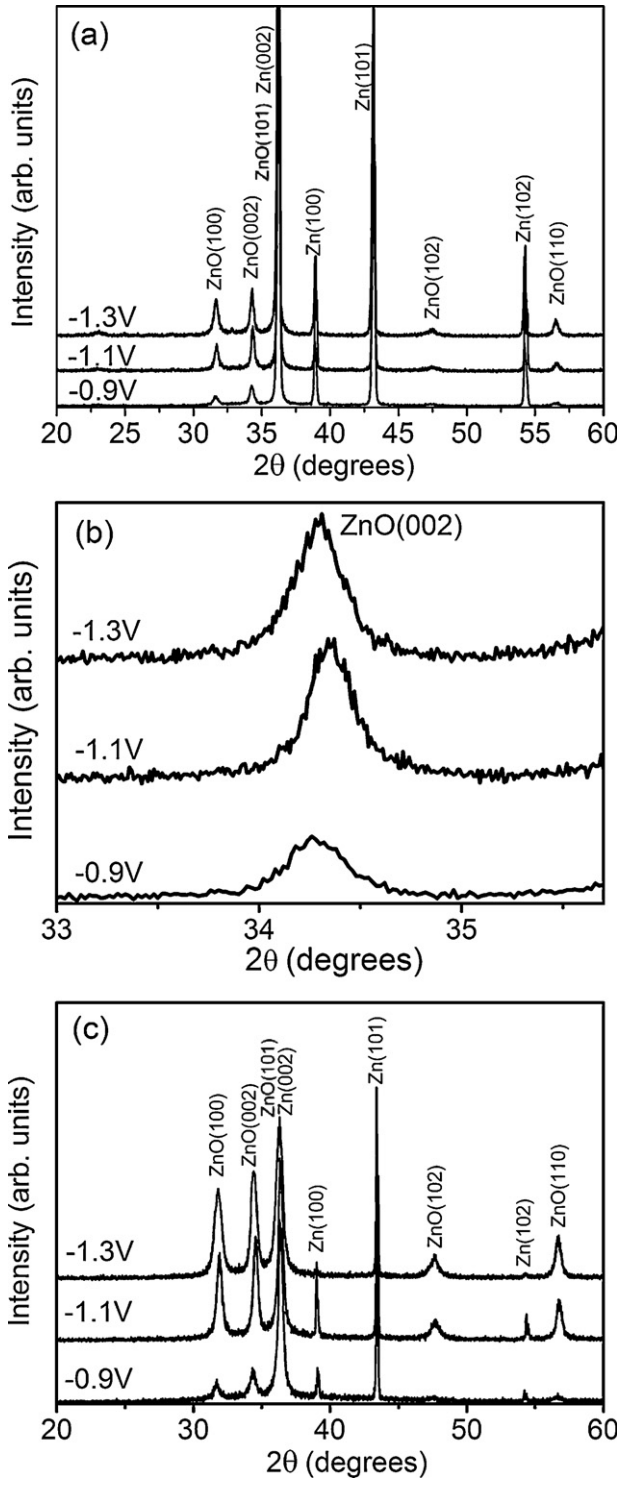

Fig. 4. (a) XRD patterns of the electrodeposited Al-doped ZnO sheets grown from the electrolyte containing 0.02 M $Zn(NO_3)_2$ and 0.001 M $Al(NO_3)_3$ at various depositing potentials. (b) The magnified XRD patterns of the (0 0 2) Bragg reflections of Al-doped ZnO sheets grown at various potentials. (c) XRD patterns of the annealed Al-doped ZnO sheets grown at various depositing potentials. The thermal annealing is treated in air ambient at 400 °C for 4 h.

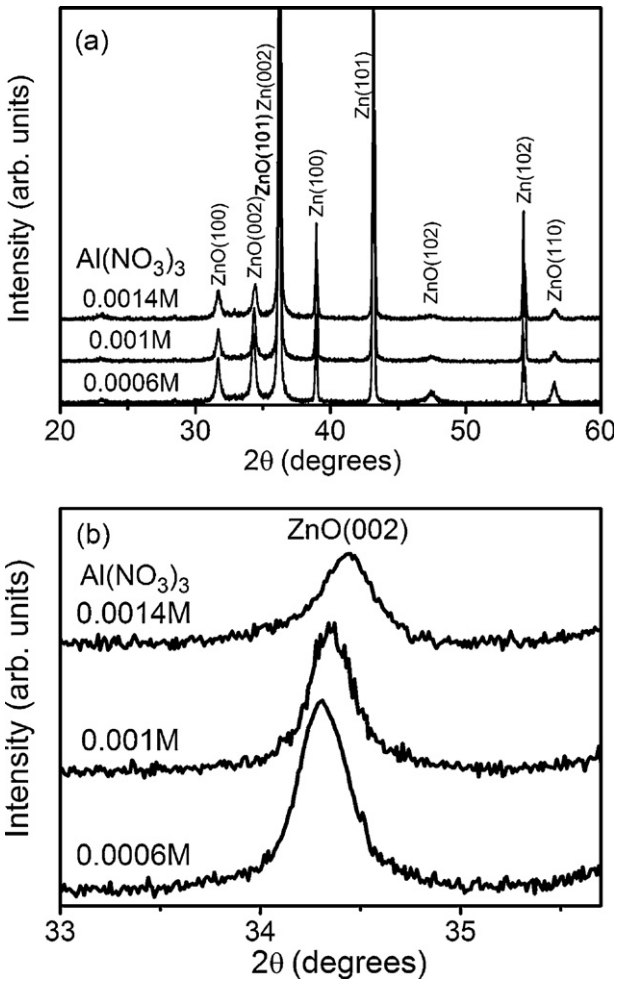

Fig. 5. (a) XRD patterns of the Al-doped ZnO sheets electrodeposited at −1.1 V from the electrolytes containing 0.02 M $Zn(NO_3)_2$ and various concentrations of $Al(NO_3)_3$. (b) The magnified XRD patterns of the (0 0 2) Bragg reflections of the Al-doped ZnO sheets.

Al ions into the ZnO lattice should result in the contraction of the ZnO lattice. Although the concentration of Al in the ZnO sheets electrodeposited at −0.9 V is higher than that electrodeposited at −1.1 V, most Al ions are not incorporated into the substitutional sites of the ZnO cells for the oxide sheets electrodeposited at −0.9 V. This results in a relatively low angle position of the Bragg reflection with respect to that electrodeposited at −1.1 V. The Al-doped ZnO sheets electrodeposited at −1.3 V shows a lower angle shift of the Bragg reflection of ZnO due to the lower content of Al in the ZnO lattice with respect to that electrodeposited at −1.1 V. By contrast, the intensity of the Bragg reflections of the annealed Al-doped ZnO sheets was markedly improved through the thermal annealing, as exhibited in Fig. 4(c). This is due to the improvement of the crystalline quality of the annealed Al-doped ZnO sheets. To identify the effect of Al concentration on the peak shift of the ZnO Bragg reflections, an electrolyte of 0.02 M $Zn(NO_3)_2$ was added with various concentrations (0.0006–0.0014 M) of $Al(NO_3)_3$. The XRD patterns in Fig. 5 show that the angular position of the Bragg reflections of the Al-doped ZnO electrodeposited at −1.1 V shifts to a higher angle with the increase of the concentration of $Al(NO_3)_3$. The increase of $Al(NO_3)_3$ concentration in the electrolyte increases the amount of Al in the ZnO, further reducing the lattice size of

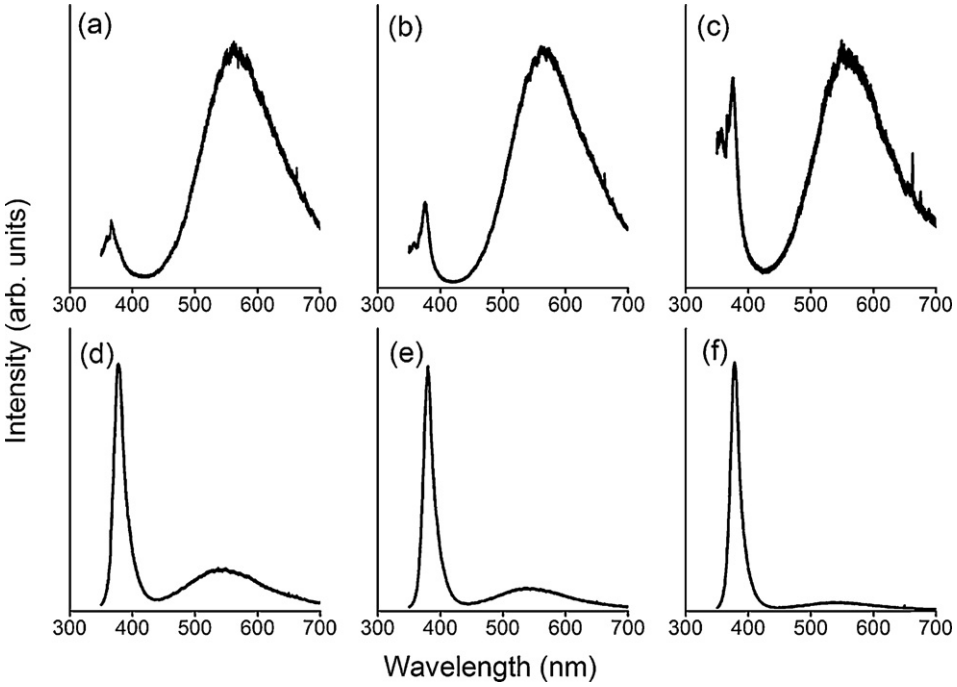

Fig. 6. PL spectra of the electrodeposited Al-doped ZnO sheets grown at various depositing potentials without and with thermal annealing: (a) −0.9 V, (b) −1.1 V, (c) −1.3 V, (d) −0.9 V with thermal annealing, (e) −1.1 V with thermal annealing, and (f) −1.3 V with thermal annealing.

ZnO and lowering the peak intensity of the Bragg reflections of ZnO.

Fig. 6 exhibits the PL spectra of the Al-doped ZnO sheets electrodeposited at various potentials with and without thermal annealing. Notably, two emission peaks are observed in the PL spectra of the Al-doped ZnO sheets; that is, the UV and visible emission peaks. The UV emission has been assigned to the near band edge emission, which originated from the direct recombination of the free excitons through an exciton-to-exciton collision process. Moreover, the appearance of the visible emission is associated with the deep level emission due to the structural disorder in the ZnO crystals. From observing Fig. 6, the weakening of the UV emission with the decreasing electrodepositing potential can be ascribed to the poor crystalline of the Al-doped ZnO nanosheets. Furthermore, the higher electrodepositing potential facilitates the larger crystals of the ZnO sheets, thus favoring a decrease of the concentration of nonradiative recombination centers. The UV emission of the annealed Al-doped ZnO sheets is enhanced and the UV-to-visible emission ratio is increased (Fig. 7) due to the improvement of crystalline quality by annealing. An increase in the UV-to-visible emission ratio via proper thermal annealing procedures was associated with the reduced concentration of structural defects [23].

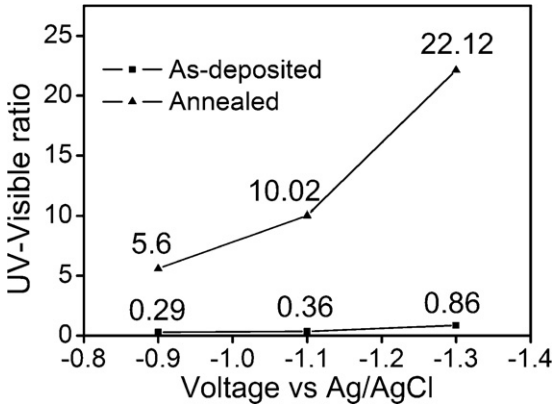

Fig. 7. UV to visible intensity ratio of PL spectra for the Al-doped ZnO sheets grown at various depositing potentials without and with thermal annealing.

4. Conclusions

Al-doped ZnO sheets were grown on polycrystalline zinc foils using cathodic electrodeposition at various potentials in an aqueous solution consisting of 0.02 M $Zn(NO_3)_2$ and 0.001 M $Al(NO_3)_3$ at 90 °C. The higher electrodepositing potential results in the Al-doped ZnO sheets having a larger lateral dimension and thickness. Moreover, the Al content in the ZnO matrix decreases according to applied potential. The XRD results show the change of the ZnO lattice size due to the Al doping effect. The crystalline quality of the Al-doped ZnO sheets was improved by thermal annealing; however, the annealing procedure roughened the appearance of the Al-doped ZnO sheets. The photoluminescent properties indicate that the Al-doped ZnO sheets electrodeposited at −1.3 V with subsequent thermal annealing at 400 °C in ambient air for 4 h are highly crystallized and of satisfactory optical quality.

Acknowledgements

This work is supported by the National Taiwan Ocean University (Grant No. NTOU-RD-AA-2010-104031) and the

National Science Council of the Republic of China (Grant No. NSC 99-2221-E-019- 055).

References

[1] Y. Sun, K.E. Addison, M.R. Ashfold, Growth of arrays of Al-doped ZnO nanocones by pulsed laser deposition, Nanotechnology 18 (2007) 495601–495604.
[2] S. Huang, Q. Xiao, H. Zhou, D. Wang, W. Jiang, Hydrothermal synthesis and conductive properties of Al-doped ZnO rod-like whiskers, J. Alloys Compd. 486 (2009) L224.
[3] Y.W Song, S.Y. Lee, Morphology-controlled one-dimensional ZnO nanostructures with customized Ga-doping, Thin Solid Films 518 (2009) 1323–1325.
[4] J.F. Chang, H.H. Kuo, I.C. Leu, M.H. Hon, The effects of thickness and operation temperature on ZnO:Al thin film CO gas sensor, Sens. Actuators B 84 (2002) 258–264.
[5] R.R. Piticescu, R.M. Piticescu, C.J. Monty, Synthesis of Al-doped ZnO nanomaterials with controlled luminescence, J. Eur. Ceram. Soc. 26 (2006) 2979–2983.
[6] M. Law, L.E. Greene, J.C. Hohnson, R. Saykally, P. Yang, Nanowire dye-sensitized solar cells, Nature 4 (2005) 455–459.
[7] V. Khranovskyy, A. Ulyashin, G. Lashkarev, B.G. Svensson, R. Yakimova, Morphology, electrical and optical properties of undoped ZnO layers deposited on silicon substrates by PEMOCVD, Thin Solid Films 516 (2008) 1396–1400.
[8] C. Yan, D. Xue, L. Zou, A solution-phase approach to the chemical synthesis of ZnO nanostructures via a low-temperature route, J. Alloys Compd. 453 (2008) 87–92.
[9] M. Wang, C.H. Ye, Y. Zhang, G.M. Hua, H.X. Wang, M.G. Kong, L.D. Zhang, Synthesis of well-aligned ZnO nanorod arrays with high optical property via a low-temperature solution method, J. Cryst. Growth 291 (2006) 334–339.
[10] X. Wang, J. Song, Z.L. Wang, Single-crystal nanocastles of ZnO, Mater. Phys. Lett. 424 (2006) 86–90.
[11] M. Fu, J. Zhou, Mechanism of the electrodeposition of ZnO nanosheets below room temperature, J. Electrochem. Soc. 157 (2010) D450–D453.
[12] S.K. Min, R.S. Mane, O.S. Joo, T. Ganesh, B.W. Cho, S.H. Han, Upright-standing ZnO nano-sheets growth using wet chemistry, Curr. Appl. Phys. 9 (2009) 492–495.
[13] L. Xu, Y. Guo, Q. Liao, J. Zhang, D.S. Xu, Morphological control of ZnO Nanostructures by electrodeposition, Phys. Chem. B 109 (2005) 13519–13522.
[14] Q. Xiao, S. Huang, J. Zhang, C. Xiao, X. Tan, Sonochemical synthesis of ZnO nanosheet, J. Alloys Compd. 459 (2008) L118.
[15] H.Y Yang, S.H. Lee, T.W. Kim, Effect of zinc nitrate concentration on the structural and the optical properties of ZnO nanostructures, Appl. Surf. Sci. 256 (2010) 6117–6120.
[16] B. Illy, B.A. Shollock, J.L. MacManus-Driscoll, M.P. Ryan, Electrochemical growth of ZnO nanoplates, Nanotechnology 16 (2005) 320–324.
[17] F. Wang, R. Liu, A. Pan, L. Cao, K. Cheng, B. Xue, G. Wang, Q. Meng, J. Li, Q. Li, Y. Wang, T. Wang, B. Zou, The optical properties of ZnO sheets electrodeposited on ITO glass, Mater. Lett. 61 (2007) 2000–2003.
[18] M. Kemell, F. Dartigues, M. Ritala, M. Leskelä, Electrochemical preparation of In and Al doped ZnO thin films for $CuInSe_2$ solar cells, Thin Solid Films 434 (2003) 20–23.
[19] R. Cebulla, R. Weridt, K. Ellmer, Al-doped zinc oxide films deposited by simultaneous rf and dc excitation of a magnetron plasma: relationships between plasma parameters and structural and electrical film properties, J. Appl. Phys. 83 (1998) 1087–1095.
[20] J.A. Taylor, An XPS study of the oxidation of AlAs thin films grown by MBE, J. Vac. Sci. Technol. 20 (1982) 751–755.
[21] L.J. Li, H. Deng, L.P. Dai, J.J. Chen, Q.L. Yuan, Y. Li, Properties of Al heavy-doped ZnO thin films by RF magnetron sputtering, Mater. Res. Bull. 43 (2008) 1456–1462.
[22] S. Liang, H. Sheng, Y. Liu, Z. Hio, Y. Lu, H. Shen, ZnO Schottky ultraviolet photodetectors, J. Cryst. Growth 225 (2001) 110–113.
[23] S. Cho, J. Ma, Y. Kim, Y. Sun, G.K.L. Wong, J.B. Ketterson, Photoluminescence and ultraviolet lasing of polycrystalline ZnO thin films prepared by the oxidation of the metallic Zn, Appl. Phys. Lett. 75 (1999) 2761–2763.